

# Designing Ionic Materials Through Multiobjective Genetic Algorithms

R. SREEVATHSAN<sup>1</sup>, B. BHATTACHARYA<sup>2</sup>, AND N. CHAKRABORTI<sup>1</sup>

<sup>1</sup>Department of Metallurgical and Materials Engineering, Indian Institute of Technology, Kharagpur, India

<sup>2</sup>Department of Civil Engineering, Indian Institute of Technology, Kharagpur, India

The present work deals with the design of ionic materials as an “inverse problem” where we determine suitable interionic distance to arrive at the desired properties. Specifically, we design ionic materials with high fracture toughness, low density, and high thermodynamic stability. Fracture toughness of the material is determined through molecular dynamics simulations, and the three conflicting objectives are optimized using multiobjective Genetic Algorithms. Two typical lattice systems, namely, the NaCl (B1) structure and the CsCl (B2) structure, are studied. The interionic potential is modeled by a combination of Born–Mayer and Coulomb potentials which represent the electron orbital repulsion and unlike ion attraction, respectively. Attempt has been made to develop a general framework for the design of ionic materials by Genetic Algorithms.

**Keywords** Born–Mayer potential; Coulomb potential; Evolutionary algorithms; Fracture toughness; Genetic algorithms; Inverse problem; Ionic materials; Lightness; Materials design; Multiobjective optimization; Pareto-problem; Thermodynamic stability.

## 1. INTRODUCTION

The applications of ionic materials are of considerable importance in numerous scientific and engineering applications. Design of ionic materials by interionic potential has been done extensively [1, 2], while the potential use of Genetic Algorithms in materials design is well illustrated by recent work in this emerging area [3–7]. This study also involves atomic simulation of crack extension [8] and is a continuation of our previous work [9] which deals with the design of simple cubic materials using Lennard–Jones interatomic potentials and multiobjective Genetic Algorithms [10]. In this study, by combining the strength of Genetic Algorithms in solving problems with conflicting objectives and the idea of ionic materials design by interatomic potential, we tried to develop materials that are high in fracture toughness, and at the same time light and thermodynamically stable. Potentially, a material this way could find extensive applications as electrode materials which are subjected to cracking and subsequent stress related failure.

The problem in the mathematical sense is an “inverse problem,” where we would fix the required material properties and look for a suitable lattice parameter catering to it. The three conflicting objectives are optimized using Nondominated Sorting Genetic Algorithm (NSGA II)—a well-known multiobjective optimization algorithm [11]. The optimization problem and evolutionary technique are elaborated in the following sections.

## 2. OPTIMIZATION PROBLEM

For an ionic material, fractures toughness, lightness, and energy are simultaneously optimized in this study.

This leads to a Pareto problem with conflicting objectives where the solution is not unique and represents the best possible tradeoffs between the objectives [10]. The problem is formulated as

1. Maximization of fracture toughness.
2. Maximization of volume (for a given mass). This is the same as maximizing the lightness and minimizing the density.
3. Minimization of energy of the system to make it thermodynamically stable.

Two cubic crystal structures were selected here for the ease of preliminary studies. Those are

- i. NaCl – B1 lattice structure (Face Centered Cubic);
- ii. CsCl – B2 lattice structure (Simple Cubic).

An *elitist* version of NSGA II was used with the Simulated Binary Crossover (SBX) [11] fixing the probability of crossover at 0.9. A real parameter mutation was used where the mutation probability was kept as 0.5. The population size was 500, and the computations were carried out for 5,000 generations.

## 3. FRACTURE TOUGHNESS THROUGH MOLECULAR DYNAMICS

The potential energy for ionic materials is modeled using a combination of Born–Mayer and Coulomb potentials [1, 12, 13]. The former represents the repulsive force due to overlapping electron orbitals while the latter incorporates the attraction between unlike ions. The total energy is expressed as

$$E(r) = Z\lambda e^{-\frac{r}{\rho}} - \frac{\alpha q_1 q_2}{4\pi\epsilon_0 r} + \frac{3}{2}nKT \quad (1)$$

Received February 26, 2008; Accepted September 10, 2008

Address correspondence to B. Bhattacharya, Department of Civil Engineering, Indian Institute of Technology, Kharagpur 721 302, WB, India; E-mail: baidurya@iitkgp.ac.in

TABLE 1.—Constants in Eq. (1).

Parameter	Description	Value	
		NaCl (B1)	CsCl (B2)
$Z$	Number of nearest neighbors	12	6
$\lambda$	Repulsive energy parameter in eV	$6.5535 * 10^3$	$8.8504 * 10^3$
$\rho$	Repulsive range parameter in Å	0.36	0.3032
$\alpha$	Madelung constant	1.747558	1.76267
$q_1, q_2$	Charge of cation and anion in esu	$\pm 4.8e^{-10}$	
$K$	Boltzmann's constant	$8.617 * 10^{-5}$ eV/K	

where the first two terms, representing the Born–Mayer and Coulomb potentials, constitute the potential energy while the last term represents the kinetic energy.  $T$  is the absolute temperature and the remaining parameters [12] are explained in Table 1. The cut-off radius,  $r_c$ , is taken to be the same for both potentials and equals  $r_c = 4.5r$  in this study, where  $r$  is the interionic distance of separation. The interionic separation was treated as the independent variable and was generated randomly within the bounds (2.25 to 3 Å for NaCl and 1.75 to 2.5 Å for CsCl) by Genetic Algorithms.

The fracture toughness of the material is computed by molecular dynamics using the Large Scale Atomic/Molecular Massively Parallel Simulator (LAMMPS) [14], by studying the onset of fracture in a precracked specimen under constant rate of loading. The effects of temperature, initial crack length, and loading rate have also been studied for varying interionic distance ( $r$ ), which remains the common variable for all the three objectives that are optimized.

The domain of simulation is a rectangular parallelepiped of dimensions  $400 \text{ Å} \times 200 \text{ Å} \times 10 \text{ Å}$  (Fig. 1). Boundary conditions are *shrink wrapped* in all directions, meaning that the simulation domain moves concomitantly with the strained lattice (no periodic boundary condition in any direction). The system is an NPT ensemble (number of atoms, pressure, and temperature are kept constant). The interatomic potential is given by the sum of Born–Mayer and Coulomb potentials as described above. Loading on the specimen is displacement-controlled: one face ( $10 \text{ Å} \times$

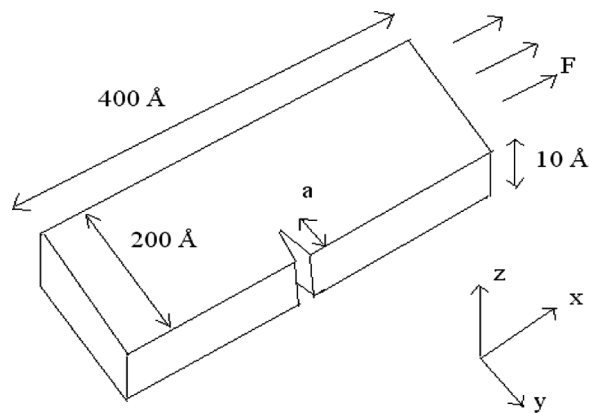


FIGURE 1.—Specimen and load configuration used to determine fracture toughness.

$200 \text{ Å}$ ) is kept stationary, the layer of atoms on its opposite face are moved axially at a constant speed so as to deform the whole lattice. The Verlet algorithm [15] is used for time integration. A crack is formed in the domain by cutting off the interaction potential between two adjacent planes [8].

For brittle and semibrittle materials, the stress intensity factor

$$K_I = Y\sigma\sqrt{\pi a} \quad (2)$$

defines the state of stress around the crack tip, where  $\sigma$  is the far-field stress,  $a$  is the crack length (in case of edge cracks), and  $Y$  is a geometric correction factor for finite sized specimens. For an edge crack, the correction factor is [16]

$$Y = 1.19 - 0.41\left(\frac{a}{w}\right) + 18.7\left(\frac{a}{w}\right)^2 - 38.48\left(\frac{a}{w}\right)^3 + 53.85\left(\frac{a}{w}\right)^4 \quad (3)$$

where  $w$  is the specimen width.

Figure 2 shows the visualization of crack formed in the lattice by the absence of interaction between two adjacent planes of atoms. This precracked specimen marks the beginning of fracture mechanics study by molecular dynamics. Figure 2 shows a section of the specimen enlarged to make the crack easily visible.

Brittle fracture takes place as soon as the drop in elastic strain energy and/or the energy supplied by external forces, for a small increment in crack length, equals the energy required to create the corresponding new crack surface. Brittle fracture proceeds catastrophically beyond this point. The energy-time history obtained through molecular dynamics simulation shows a sharp drop at this point of unstable fracture. The stress intensity factor at this point equals  $K_c$ , the fracture toughness, which is a temperature- and thickness-dependent quantity [16]. For purely brittle materials,  $K_c$  is independent of crack length.

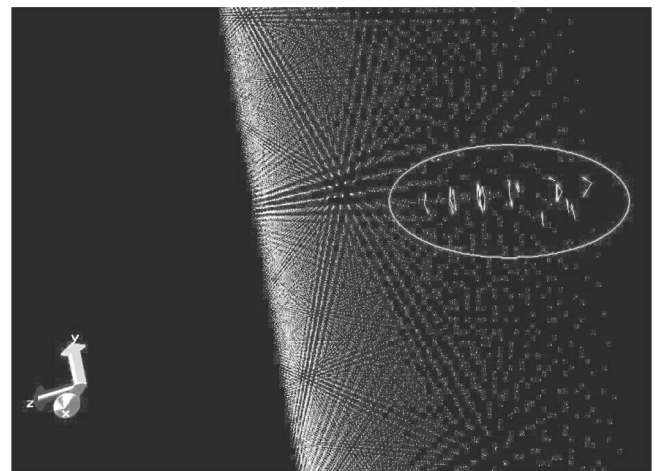


FIGURE 2.—Configuration of the simulated precracked specimen. Crack formed is shown.

In this study, fracture toughness is obtained for various crack lengths and interionic distances. The effects of temperature and loading rate are also investigated. For a given combination of crack length ( $a$ ), temperature ( $T$ ), loading rate ( $v$ ), and interionic distance ( $r$ ), the critical force at the onset of unstable fracture ( $F_c$ ) is identified from the simulated force-time history. The fracture toughness is then given as

$$K_c(T, r, v) = Y(a) * \left(\frac{F_c}{A}\right) * \sqrt{\pi a} \quad (4)$$

where  $A$  is the cross-sectional area.

After fracture toughness, the evaluation of the two remaining objectives is a rather straight forward task. The volume,

$$V = a_L^3 \quad (5)$$

for both simple cubic and FCC system, where the lattice parameter  $a_L$  is related to the equilibrium interatomic spacing  $r$  as  $a_L = \sqrt{2}r$  for FCC lattice, and  $a = r$  for simple cubic structure. The calculation of volume is trivial since the lattice of both NaCl and CsCl consists of two interlocked FCC and simple cubic structures, respectively. Since the mass of molecules in a unit cell for each case is constant, density can be calculated from the mass and volume calculated from Eq. (5).

The objective function for energy was directly computed from Eq. (1).

## 4. RESULTS AND DISCUSSION

### 4.1. Molecular Dynamics Calculations

From molecular dynamics calculations we obtain the time histories of displacement, energy, and force applied on the system. A few examples are described for better understanding of the procedure for determination of the fracture stress which forms the basis of our fracture toughness calculation.

Figure 3(a) shows uniform displacement with time (i.e., constant loading rate). From the plot of energy time history [Fig. 3(b)], the instant at which catastrophic failure occurs can be identified, and hence the corresponding critical force can be obtained [17, 18] [Fig. 3(c)]. Fracture toughness can be found using Eq. (1).

### 4.2. Temperature and Crack Length Dependence Study

The temperature dependence of the fracture toughness is now investigated. Three different temperatures 1 K, 298 K, and 500 K are selected, and the results for NaCl and CsCl systems are given below (Table 2 and its graphical version

TABLE 2.—Temperature dependence of  $K_c$  at different crack lengths for NaCl lattice.

Crack length in Å for a specimen width of 200 Å	$K_c$ in MPa√m at different temperatures for NaCl (K)			$K_c$ in MPa√m at different temperatures for CsCl (K)		
	1	298	500	1	298	500
10	1.675	1.79	1.899	0.915	1.024	1.153
15	1.774	1.92	2.066	0.9088	1.02	1.1832
20	1.683	1.797	1.97	0.9594	1.025	1.1567
30	1.89	2.04	2.28	0.9309	1.06	1.285

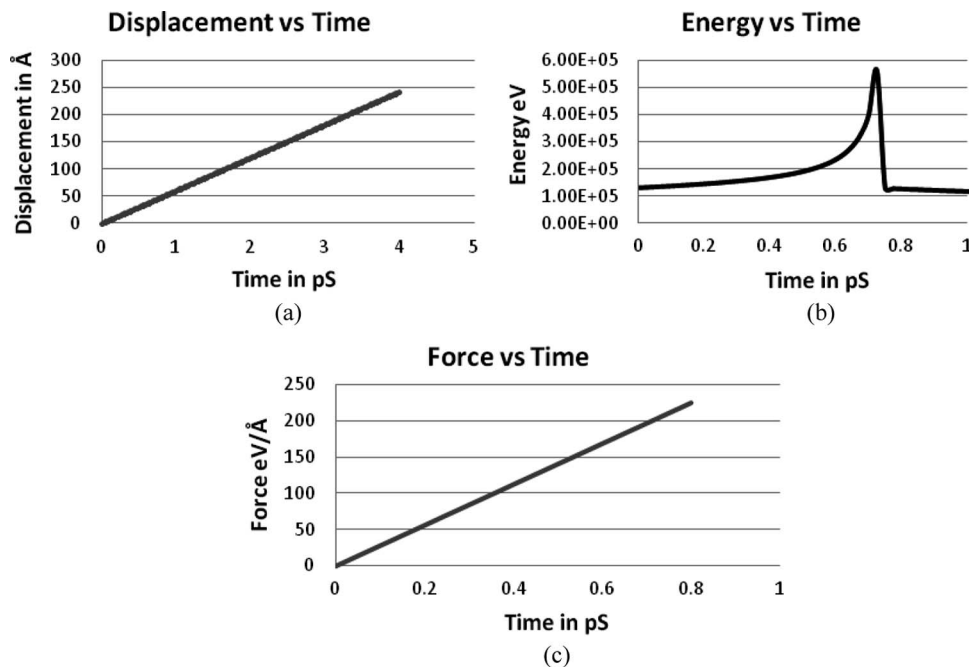


FIGURE 3.—Typical plots showing time histories of displacement, total energy and force.

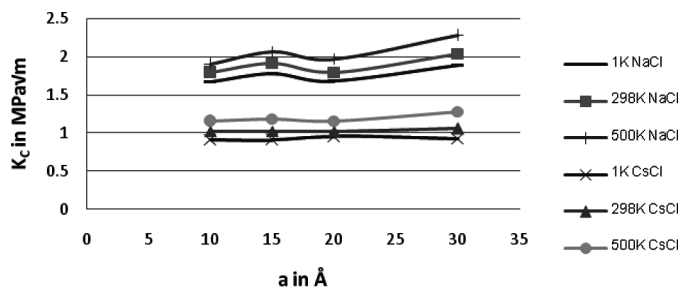


FIGURE 4.— $K_c$  vs.  $a$  at different temperatures for NaCl and CsCl structures.

TABLE 3.—Loading rate dependence of  $K_c$  at different crack lengths for NaCl lattice.

Crack length in Å for a specimen width of 200 Å	$K_c$ in MPa√m at different loading rates for NaCl (Å/pS)			$K_c$ in MPa√m at different loading rates for CsCl (Å/pS)		
	45	60	80	25	35	50
10	1.695	1.63	1.67	0.922	0.942	0.915
15	1.81	1.75	1.775	0.9517	0.9614	0.9088
20	1.786	1.73	1.683	0.99	0.992	0.9594
30	1.99	1.96	1.895	0.975	0.997	0.9309

Note: 1 Å/pS = 100 m/s.

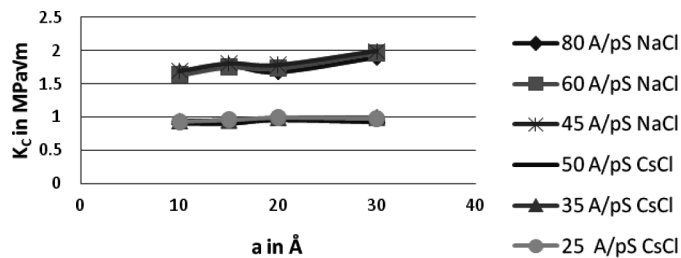


FIGURE 5.— $K_c$  vs.  $a$  at different loading rates for NaCl and CsCl structures at 298 K.

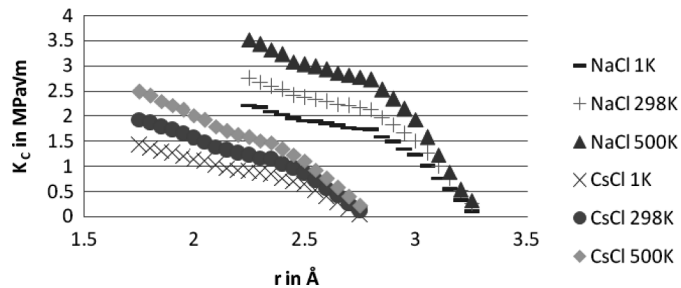


FIGURE 6.—Fracture toughness vs. interionic distance at different temperatures.

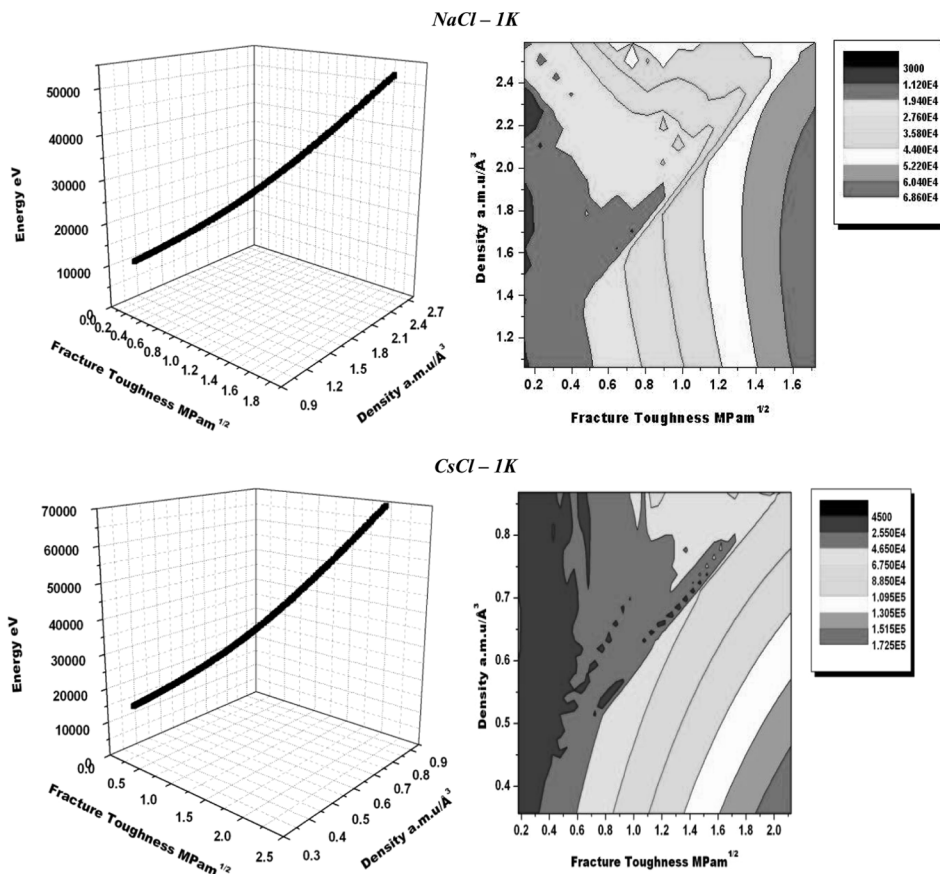


FIGURE 7.—Pareto-frontiers and energy contour plots of NaCl and CsCl at 1 K.

Fig. 4). It is clear that  $K_c$  is largely indifferent to crack length thus confirming that the fracture is brittle (although there is a hump around  $a = 15 \text{ \AA}$  which we suspect is due to the finite width of the specimen slab). The increase in fracture toughness with temperature is clear from the figure, as more energy is needed for crack propagation at higher temperatures.

4.3. Effect of Loading Rate on  $K_c$

The effect of loading rate on fracture toughness is studied, and the results given below.

Table 3 and its counterpart, Fig. 5 show the relation between  $K_c$  and  $a$  at different loading rates at constant temperature of 298 K. We have made sure that the speeds used in this study are less than half the Rayleigh wave speed,  $R_n$ , in the given material, which is the limiting speed of sound in a continuum solid [19]. The Rayleigh wave speeds ( $R_n = \sqrt{\frac{E}{\rho}}$  where  $E$  = elastic modulus and  $\rho$  = density) in NaCl and CsCl are  $18340 \text{ m s}^{-1}$  and  $11530 \text{ m s}^{-1}$ , respectively [20].

From Fig. 5 it is clear that fracture toughness is largely independent of the loading rate; and we have already shown (Fig. 4) that fracture toughness is largely insensitive to crack length as well. Hence, we find that  $K_c$  depends mainly on temperature, and in the subsequent optimization study, we

investigate the variations in the three conflicting objectives at three levels of temperature: 1 K, 298 K, and 500 K.

4.4. Fracture Toughness as a Function of Interionic Separation Distance

Figure 6 presents the objective function of fracture toughness as a function of the independent variable,  $r$ , at various temperatures for both materials. The loading rate for NaCl is  $60 \text{ \AA/ps}$ , and that for CsCl is  $35 \text{ \AA/ps}$ . The increase in  $r$  causes decrease of fracture toughness, and when  $r$  gets closer to cutoff radius, the fracture toughness falls very close to zero in both cases. The rapid change in the slope of  $K_c$  vs.  $r$  plot can be explained by the rapid drop in interaction energy between ions as the value of  $r$  approached cutoff radius.

To evaluate the first objective,  $K_c$ , for different randomly generated independent variable  $r$ ; intermediate values are linearly interpolated as

$$K_c = K_i + \frac{(r - r_i)}{(r_{i+1} - r_i)}(K_{i+1} - K_i) \tag{6}$$

where  $K_i, K_{i+1}$  and  $r_i, r_{i+1}$  are two consecutive values of fracture toughness and interionic distances, respectively.  $K_c$  represents the interpolated value of fracture toughness.

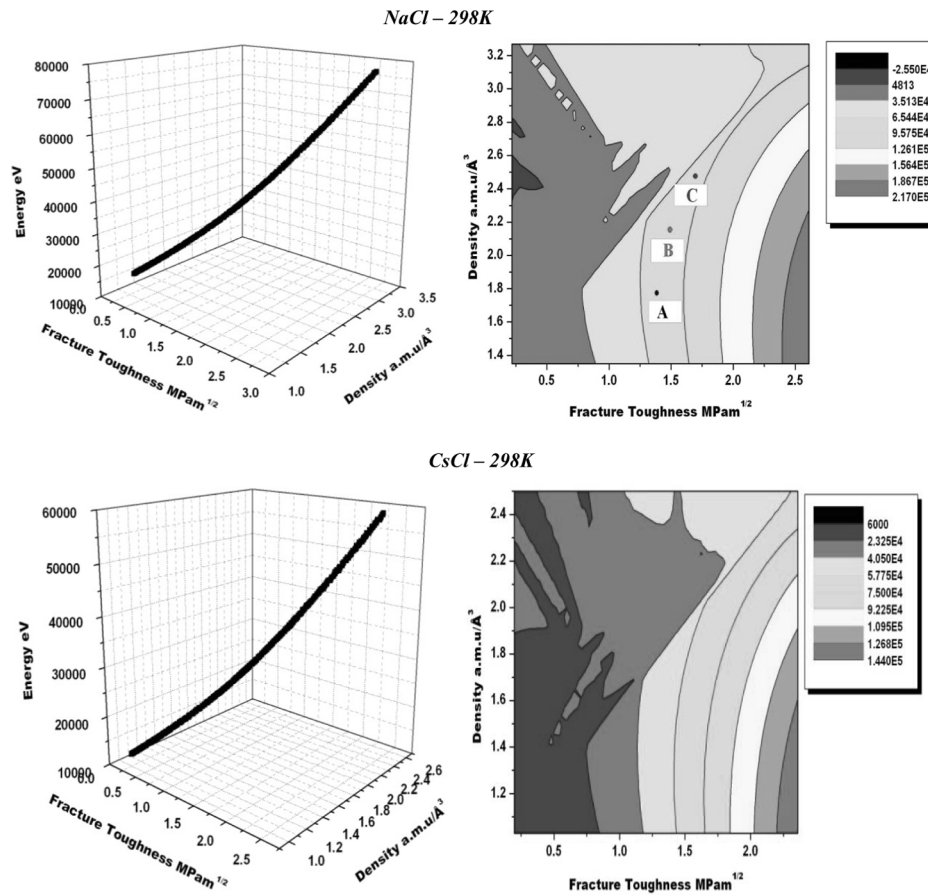


FIGURE 8.—Pareto-frontiers and energy contour plots of NaCl and CsCl at 298 K.

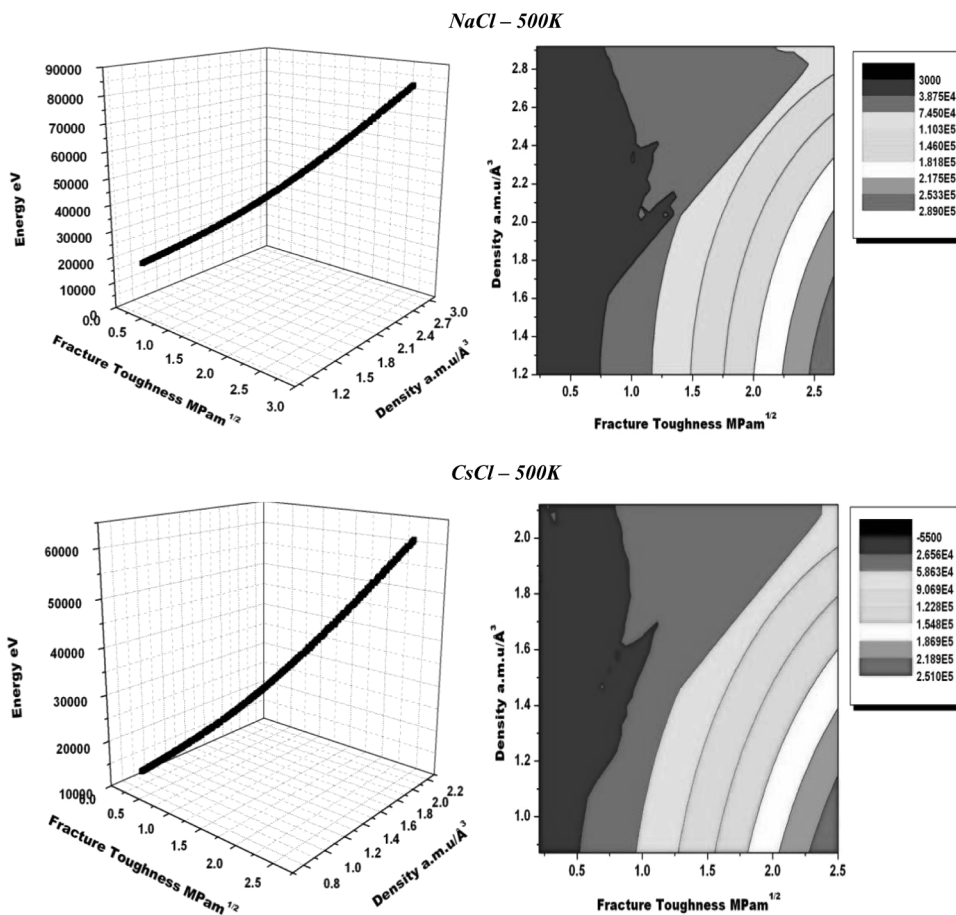


FIGURE 9.—Pareto-frontiers and energy contour plots of NaCl and CsCl at 500 K.

#### 4.5. Optimization of Conflicting Objectives

As mentioned before, the three objectives—high fracture toughness, low density, and low energy—are conflicting, and in this section we present the Pareto frontier and its various cross-sections involving these three objectives. The effect of temperature on the Pareto frontier is investigated at three levels: 1 K, 298 K, and 500 K. As also stated previously, the optimization of the three objectives is performed with a single independent variable,  $r$ .

Figures 7–9 present, on the left column, the Pareto frontiers for B1(NaCl) and B2(CsCl) lattices at the three different temperatures. In the right column, cross-sections of the Pareto frontier at various values of optimal energy are presented as contour plots.

From both NaCl and CsCl plots it is clearly visible that high optimal fracture toughness can be designed by varying  $r$ : the cost is higher energy and/or higher density. The same way, lower density can be achieved by either settling for low fracture toughness with high thermodynamic stability (on one extreme), or going for a high fracture toughness that only comes with decreased thermodynamic stability (on the other extreme); of course, any other compromise with intermediate values may also be made.

The above point is illustrated in Fig. 8; note the 3 points of reference A, B, and C for NaCl at 298 K. At similar

energy levels, the attainment of better fracture toughness, i.e., from A to B and B to C can be achieved only by a compromise in density which increases.

Figure 10 shows typical plots of individual property correlations at the fixed value of the other objective. This reiterates the conflicting nature of the objectives: energy has to increase to attain better fracture toughness while the density also gets higher which is not desirable. Hence the use of genetic algorithms helps design new materials that are optimal in all the three objectives, denoting the best possible tradeoffs between them.

The choice between the two materials NaCl and CsCl can be made in accordance with the user's requirement. The above results seem to indicate that CsCl, for a given fracture toughness (say 1 MPa $\sqrt{m}$ , Fig. 8), has better density and energy combination than does NaCl (1 a.m.u./Å<sup>3</sup> and 32000 eV for CsCl compared to 1.4 a.m.u./Å<sup>3</sup> and 50000 eV for NaCl). Alkali halide fibers of high impact resistance find potential applications in infrared fibers for laser power delivery. They have come up as potential replacements of conventional silica fibers with the advantage of having very low power losses [21]. If fracture toughness is one of the main objectives of such application, CsCl crystal would clearly win over its NaCl counterpart.

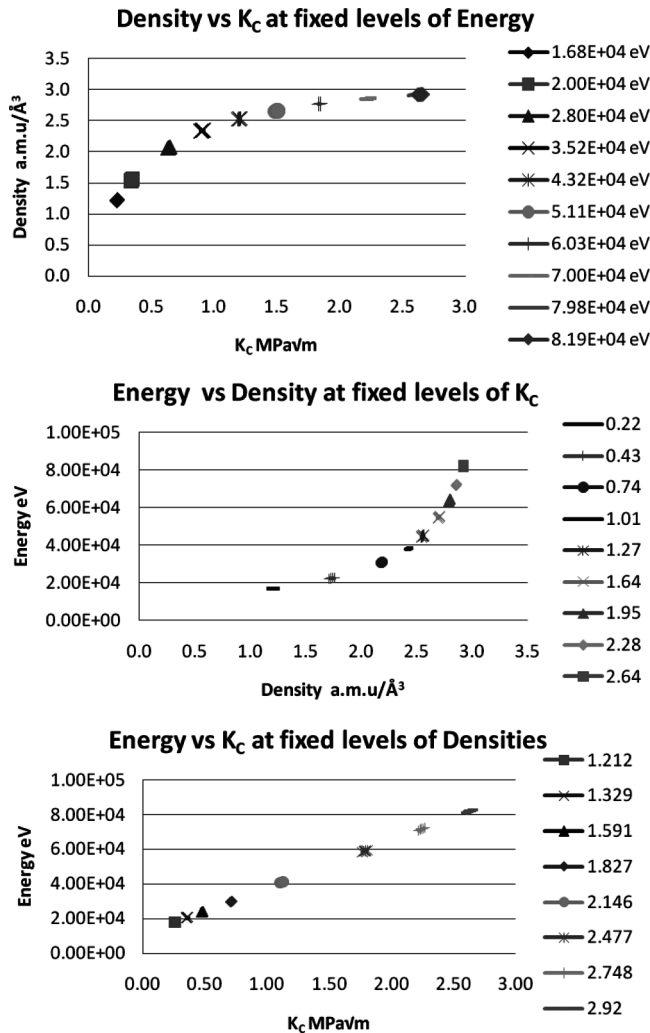


FIGURE 10.—Typical plots of individual optimized property correlations showing NaCl at 298 K.

## 5. CONCLUDING REMARKS

The work has illustrated the potential use of multiobjective genetic algorithms in solving inverse problems, based on interatomic potentials, where we derived the interionic separation for required mechanical and physical properties. The conflicting objectives are optimized to produce a Pareto-frontier leaving the designer with flexibility in material selection. Of course, the examples shown here do not lead to any “new” material design since we start with two known ionic materials and play with their interionic separation to vary the objective values—the purpose was simply to demonstrate the methodology. The next step would be to allow the potential model parameters (Eq. 1), masses of the two species, and the interionic separation to vary which would take us closer to the actual design of new materials. Work is already under way.

## REFERENCES

- Murrell, J.N.; Tennyson, J. Many-body contributions to the intermolecular potential in alkali halide crystals and clusters. *Mol. Phys.* **1981**, *42*, 747–755.
- Kendrick, J.; Mackrodt, W.C. Interatomic potentials for ionic materials from first principles calculations. *Solid State Ionics* **1983**, *8*, 247–253.
- Babu, B.V.; Mubeen, J.H.S.; Chakole, P.G. Simulation and optimization of wiped-film poly-ethylene terephthalate (PET) reactor using multiobjective differential evolution (MODE). *Mater. Manuf. Process.* **2007**, *22*, 541–552.
- Sastry, K.; Johnson, D.D.; Thompson, A.L.; Goldberg, D.E.; Martinez, T.J.; Leiding, J.; Owens, J. Optimization of semi-empirical quantum chemistry methods via multiobjective Genetic Algorithms: Accurate photodynamics for larger molecules and longer time scales. *Mater. Manuf. Process.* **2007**, *22*, 553–561.
- Saxén, H.; Pettersson, F.; Gunturu, K. Evolving nonlinear time-series models of the hot metal silicon content in the blast furnace. *Mater. Manuf. Process.* **2007**, *22*, 577–584.
- Mitra, K.; Majumdar, S. Multicriteria optimal control of polypropylene terephthalate polymerization reactor. *Mater. Manuf. Process.* **2007**, *22*, 532–540.
- Sahay, S.S.; Mehta, R.; Krishnan, K. Genetic-algorithm-based optimization of an industrial age-hardening operation for packed bundles of aluminum rods. *Mater. Manuf. Process.* **2007**, *22*, 615–622.
- Kanninen, M.F.; Gehlen, P.C. Atomic simulation of crack extension in BCC iron. *Journal of Fracture Mechanics* **1971**, *7*, 471–474.
- Chakraborti, N.; Sreevathsan, R.; Jayakanth, R.; Bhattacharya, B. Tailor-made materials design: An evolutionary approach using multi-objective genetic algorithms. *Comp. Mater. Sci.* **2009**, in press. doi: 10.1016/j.commatsci.2008.03.057
- Miettinen, K. *Non-Linear Multiobjective Optimization*; Kluwer Academic Publishers: Norwell, 1999.
- Deb, K. *Multi-Objective Optimization by Evolutionary Algorithms*; John Wiley & Sons: Chichester, 2001.
- Ghosh, A.; Basu, A.N. A unified study of the lattice statics and dynamics of the cesium halides. *J. Phys. C. Solid State* **1976**, *9*, 4365–4374.
- Kittel, C. *Solid State Physics*; John Wiley and Sons: Chichester, 1971; 102–125.
- Allen, M.P. Introduction to molecular dynamics simulation. *Computational Soft Matter* **2004**, *23*, 1–28.
- Zhao, J.W.; Yin, X.; Liang, S.; Liu, Y.H.; Wang, D.X.; Deng, S.Y.; Hou, J. Ultra-large scale molecular dynamics simulation for nano-engineering. *Chem. Res. Chinese U* **2008**, *24*, 367–370.
- Broek, D.E. *Elementary Engineering Fracture Mechanics*; Kluwer Academic Publishers: Norwell, 1982; 75–77.
- Rottler, J.; Barsky, S.; Robbins, M.O. Cracks and crazes: on calculating the macroscopic fracture energy of glassy polymers from molecular simulations. *Phys. Rev. Lett.* **2002**, *89*, 1–5.
- Kassner, M.E.; Nasser, N.S.; Suo, Z.G.; Bao, G.; Barbour, J.C.; Brinson, L.C.; Espinosa, H.; Gao, H.J.; Granick, S.; Gumbsch, P.; Kim, K.S.; Knauss, W.; Kubin, L.; Langer, J.; Larson, B.C.; Mahadevan, L.; Majumdar, A.; Torquato, S.; Swol, F.V. New directions in mechanics. *Mech. Mater.* **2005**, *37*, 231–259.
- Abraham, F.F. How fast can cracks move? A research adventure in materials failure using millions of atoms and big computers. *Adv. Phys.* **2003**, *52*, 727–90.
- Washabaugh, P.D.; Knauss, W.G.; A reconciliation of dynamic crack velocity and Rayleigh wave speed in isotropic brittle solids. *Int. J. Fracture* **2004**, *65*, 97–114.
- Harrington, J.A. Infra-red alkali halide fibers. *Appl. Optics* **1988**, *15*, 3097–3101.